Journal of King Saud University - Science 36 (2024) 103518

HOSTED BY

Contents lists available at ScienceDirect

Journal of King Saud University - Science

journal homepage: www.sciencedirect.com

New quinazoline-N-4-fluorophenyl derivatives as potential anticancer agents: Discovery of a promising dual EGFR/VEGFR-2 inhibitor

Mohammed H. Geesi *

Department of Chemistry, College of science and humanities in Al-Kharj, Prince Sattam bin Abdulaziz University, Al-Kharj 11942, Saudi Arabia

ARTICLE INFO

Keywords:
Quinazoline
Molecular docking
MTT assay
EGFR
VEGFR-2
Tyrosine kinase

ABSTRACT

This research is dedicated to synthesizing a new group of quinazoline-N-4-fluorophenyl **4a–d** structures and evaluating their anticancer efficacy across multiple cancer cell lines. The molecular design of these derivatives was based on the structural features required for dual inhibition of VEGFR-2 and EGFR. The new derivatives were structurally characterised by NMR analyses. Cytotoxicity was assessed in this study against various cancerous cell strains. Among these, the top three products were further assessed for their capacity to block the enzymatic activity of (VEGFR-2) and (EGFR). Product **4b**, in particular, exhibited a strong cytotoxic profile, with IC_{50} values of 68.2 ± 1.54 nM against EGFR and 189 ± 5.66 nM against VEGFR-2. Molecular docking studies demonstrated that compound **4b** effectively interacts with the active sites of both VEGFR-2 and EGFR, potentially influencing its action pathway as a powerful inhibitor.

1. Introduction

A broad category of critical and complicated diseases falls under the umbrella of cancer. According to statistics published by the WHO, nearly nine million cancer-related deaths were recorded in 2020. The same source predicts that the number of cancer cases could exceed 12 million by 2030 (Bray et al., 2021). Current research focuses on developing innovative approaches to target specific signalling pathways in order to eradicate the negative aspects of conventional chemotherapy in cancer treatment (Liu et al., 2018).

Heterocyclic derivatives that include at least one atom different from carbon particularly nitrogen, oxygen, or sulfur are often involved in the inhibition of key proteins associated with tumor growth and cellular proliferation (Kumar et al., 2023; Martins et al., 2015; Tilahun et al., 2025; Peerzada et al., 2021; Drakontaeidi et al., 2024; Papanotas and Pontiki, 2024; Obaid et al., 2022). Tyrosine kinase (TK) is fundamental to growth factor signalling, as it represents a key focus in anticancer therapy. Inhibition of angiogenesis, particularly through targeting Vascular Endothelial Growth Factor Receptor VEGFR, is an important strategy for impeding tumour progression (Zahran et al., 2023). Furthermore, VEGFR is pivotal in both normal and pathological angiogenesis, rendering it a prime target for novel cancer therapies (Ghorab et al., 2017).

The aberrant expression of Vascular Endothelial Growth Factor Receptor 2 (VEGFR-2) has been detected in several types of cancer cells (colorectal and lung). Therefore, targeting VEGFR-2 is a crucial strategy in anti-angiogenic therapy (Cook and Figg, 2010). Scientists are currently engaged in developing new Type II and III inhibitors to block VEGFR-2 following sustained TK inhibition (Traxler and Furet, 1999). On the other hand, Vascular Endothelial Growth Factor (VEGF) and Epidermal Growth Factor (EGF) can independently contribute to cancer progression and resistance to treatment through overlapping signalling pathways (Panigrahy et al., 2005). The emergence of resistance to VEGFR-2 inhibitors underscores the importance of exploring novel therapeutic options (Cao et al., 2011).

The Epidermal Growth Factor Receptor (EGFR) is a crucial protein in cellular signalling and is largely responsible for the accelerated multiplication of cancer cells (Gschwind et al., 2004; Li and Li, 2014). EGFR mutations are commonly associated with reduced responsiveness to TKIs, which often leads to resistance and cancer progression (Ayati et al., 2020). One notable example is the $EGFRT^{790M}$ mutation, which increases ATP binding affinity to levels similar to the non-mutated form, thus reducing the effectiveness of TKIs in the presence of ATP (Stockley et al., 2018). Targeting EGFR, along with the VEGF pathway, has emerged as a promising strategy for enhancing therapeutic responses, particularly in cases of non-small cell lung cancer (Byers and Heymach, 2007). Suppression of VEGF signalling is pivotal in cancer treatment (Panigrahy et al., 2002), and FDA-approved small molecule inhibitors

* Corresponding author.
E-mail address: m.geesi@psau.edu.sa.

https://doi.org/10.1016/j.jksus.2024.103518
Received 6 July 2024; Received in revised form 30 October 2024; Accepted 1 November 2024
Available online 4 November 2024

like quinazoline derivatives (e.g., Vandetanib, Gefitinib) target both EGFR and VEGFR-2 pathways to inhibit tumour progression (Yu and Pao, 2013) (Fig. 1-A).

Quinazoline-based compounds, including WHI-P180, Erlotinib, Afatinib, Gefitinib, Lapatinib, and, Vandetanib are clinically significant for their ability to target EGFR and VEGFR-2 pathways and inhibit tumour growth (Abdullaziz et al., 2017). Moreover, quinazoline scaffolds are of particular interest in designing potential anticancer agents (Ghorab et al., 2018). Hybridisation strategies aimed at combining EGFR and VEGFR inhibition with other pharmacophores possessing potent antitumor activity, such as quinazolines, seem to be promising for enhancing compound efficacy (Ying et al., 2010) (Fig. 1-A).

Guided by existing literature and a thorough analysis of the proteins in question (refer to Fig. 1-B), this study centers on the insertion of new pharmacophoric groups derived from the literature on EGFR and VEGFR-2, taking into consideration their biological relationship with the quinazoline scaffold. We will develop new substituted quinazoline derivatives, using **Erlotinib** and **Sorafenib** (inhibitors of EGFR and VEGFR-2) as starting points to introduce structural modifications. The structural analysis of these derivatives has revealed the following information: a hetero-aromatic moiety to enhance affinity towards ATP (**1**), a central hydrophobic spacer (**2**), a binding site to facilitate hydrogen bonding with specific sites on the biological receptor such as Asp1046 and Glu885 (**3**), and finally, an allosteric hydrophobic group at the molecule's terminus (**4**). This design is illustrated in Fig. 1-B (Lee et al., 2010). Moreover, the quinazolinone derivatives **4a–d** developed in this research exhibit the key pharmacophoric characteristics of EGFR and VEGFR-2. The rational analysis of the SAR of Erlotinib and Sorafenib towards EGFR and VEGFR-2 has led us to introduce various substituents onto the molecules to be synthesised, including (**1**) a hydrophobic group

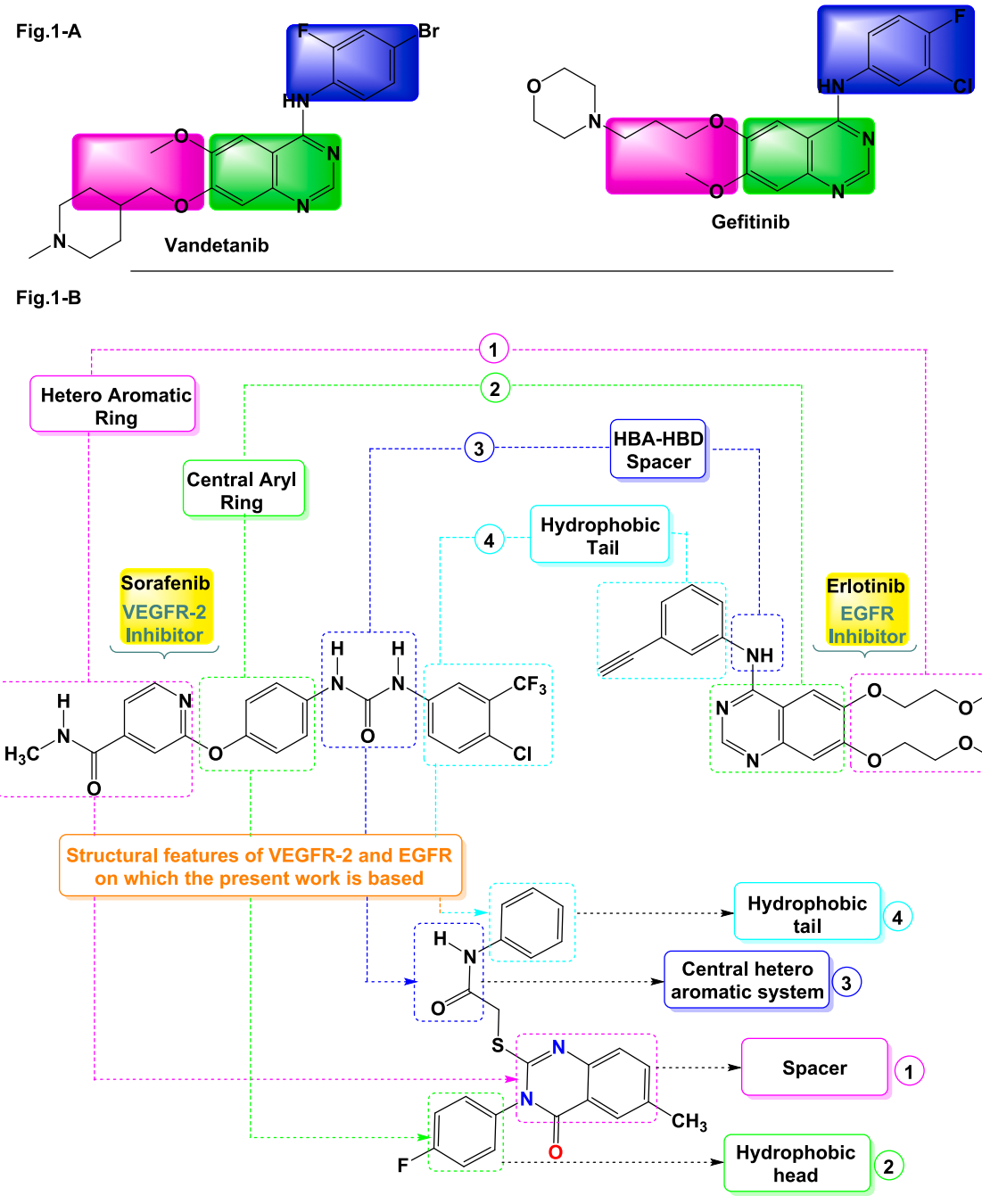

Fig. 1. Compounds (Gefitinib & Vandetanib) active against TKIs (A) and highlights the fundamental structural characteristics of VEGFR-2 and EGFR inhibitors (B).

at the molecule's terminus, (**2**) a hetero-aromatic motif to enhance affinity towards Lys721 and Met769, (**3**) an N–H spacer to facilitate hydrogen bond formation with the biological target, and (**4**) a second hydrophobic group opposite the first one (Liu et al., 2006; Soliman et al., 2019) (Fig. 1-B).

In order to expand the SAR profile of the quinazoline derivatives, a fluorine atom was introduced at the aromatic ring in para position to improve the hydrogen bonding capabilities. Additionally, modifications were made to the sulfur substitution at the C2 position by incorporating various aromatic groups. The derivatives were then subjected to incubation with multiple cancer cell lines for a 24-hour period, followed by molecular modelling studies to explore their interactions and potential effectiveness.

2. Experimental section

The compounds involved in this research were procured from Aldrich and Acros (The United States). Physical properties, such as the melting point, were determined using a Kofler bench. NMR analysis was conducted at a resolution of 500 MHz using a Bruker Avance III spectrometer.

3. Synthesis of quinazolinone 3

A combination of 0.01 mol of 2-amino-5-methylbenzoic acid **1** and 5-fluorophenyl isothiocyanate **2**, along with a few drops of Et_3N in 30 mL of ethanol, was prepared. The mixture was refluxed for approximately 2 h. The formed precipitate was filtered and recrystallized in ethanol after treatment with HCl **(**Geesi et al., 2020).

4. Synthesis of quinazolinone-N-substituted compounds 4a-d

For 10 h of stirring in acetone as the solvent, an equimolar mixture of derivative **3** (5 mmol) and acetamide derivatives or alkyl halide (added separately) was refluxed in the presence of K_2CO_3. The precipitate formed after the reaction was recrystallised in ethanol **(**Geesi, 2020; Riadi et al., 2024).

*4.1. 2-((3-(4-Fluorophenyl)-6-methyl-4-oxo-3,4-dihydroquinazolin-2-yl)thio)-N-(naphthalen-1-yl)acetamide (**4a**)*

(81 %, 173 ± 2 °C). ^{1}H NMR (500 MHz, $CDCl_3$): δ = 2.49 (s, 3H, CH_3), 3.89 (s, 2H, CH_2), 7.20 (m, 3H, HC$_{Ar}$), 7.30 (m, 2H, HC$_{Ar}$), 7.52 (d, 2H, HC$_{Ar}$), 7.58–7.67 (m, 3H, HC$_{Ar}$), 7.85 (m, 3H, HC$_{Ar}$), 8.04 (d, 1H, HC$_{Ar}$), 10.19 (s, 1H, NH). ^{13}C NMR (125 MHz, $CDCl_3$): δ = 21.08 (CH_3); 36.49 (CH_2); 116.77 (C); 116.95 (HC$_{Ar}$); 118.50 (C$_{Ar}$); 119.35 (C$_{Ar}$); 124.74 (C$_{Ar}$); 127.07 (C$_{Ar}$); 129.38 (C$_{Ar}$); 129.53 (C$_{Ar}$); 130.82 (C$_{Ar}$); 130.90 (C$_{Ar}$); 132.54 (C$_{Ar}$); 136.72 (C$_{Ar}$); 137.11 (C$_{Ar}$); 142.12 (C$_{Ar}$); 144.55 (C$_{Ar}$); 157.08 (C); 161.00 (C); 162.26 (C); 164.26 (C); 166.84 (C); 196.72 (C).

*4.2. 2-((2-(4-Bromophenyl)-2-oxoethyl)thio)-3-(4-fluorophenyl)-6-methylquinazolin-4(3H)-one (**4b**)*

$C_{23}H_{16}BrFN_2O_2S$. (84 %, 164 ± 2 °C). ^{1}H NMR (500 MHz, $CDCl_3$): δ = 2.47 (s, 3H, CH_3), 4.55 (s, 2H, CH_2), 7.14 (m, 1H, CH_{Ar}), 7.30 (m, 2H, CH_{Ar}), 7.39 (m, 2H, CH_{Ar}), 7.49 (dd, 1H, CH_{Ar}), 7.71 (m, 2H, CH_{Ar}), 7.98 (m, 2H, CH_{Ar}), 8.02 (d, 1H, CH_{Ar}). ^{13}C NMR (125 MHz, $CDCl_3$): δ = 21.10 (CH_3); 39.18 (CH_2); 116.74 (HC$_{Ar}$); 116.92 (HC$_{Ar}$); 119.25 (HC$_{Ar}$); 125.60 (HC$_{Ar}$); 126.56 (HC$_{Ar}$); 128.68 (HC$_{Ar}$); 129.86 (HC$_{Ar}$); 131.02 (HC$_{Ar}$); 131.09 (C$_{Ar}$); 135.03 (C$_{Ar}$); 136.07 (C$_{Ar}$); 136.26 (C$_{Ar}$); 145.27 (C$_{Ar}$); 154.71 (C); 161.60 (C); 164.26 (C); 192.70 (C).

*4.3. N-(4-Acetylphenyl)-2-((3-(4-fluorophenyl)-6-methyl-4-oxo-3,4-dihydroquinazolin-2-yl)thio)acetamide (**4c**)*

$C_{25}H_{20}FN_3O_3S$. (83 %, 155 ± 2 °C). ^{1}H NMR (500 MHz, DMSO-d_6): δ = 2.55 (3H, s, CH_3), 2.66 (s, 3H, CH_3), 4.25 (s, 2H, CH_2), 7.57 (m, 3H, HC$_{Ar}$), 7.72 (dd, 2H, HC$_{Ar}$), 7.76 (dd, 1H, HC$_{Ar}$), 7.87 (d, 2H, HC$_{Ar}$), 7.99 (s, 1H, HC$_{Ar}$), 8.07 (d, 2H, HC$_{Ar}$), 10.87 (s, 1H, NH). ^{13}C NMR (125 MHz, DMSO-d_6): δ = 20.57 (CH_3); 26.28 (CH_3); 37.17 (CH_2); 116.29 (HC$_{Ar}$); 116.47 (HC$_{Ar}$); 118.18 (HC$_{Ar}$); 119.11 (HC$_{Ar}$); 125.61 (HC$_{Ar}$); 125.78 (HC$_{Ar}$); 129.40 (HC$_{Ar}$); 131.69 (HC$_{Ar}$); 131.76 (C$_{Ar}$); 135.61 (C$_{Ar}$); 136.04 (C$_{Ar}$); 143.12 (C$_{Ar}$); 145.03 (C$_{Ar}$); 155.61 (C); 160.52 (C); 166.32 (C); 196.35 (C).

*4.4. 2-(Ethylthio)-3-(4-fluorophenyl)-6-methylquinazolin-4(3H)-one (**4d**)*

$C_{17}H_{15}FN_2OS$. (78 %, 159 ± 2 °C). ^{1}H NMR (500 MHz, $CDCl_3$): δ = 1.35 (t, 3H, CH_3), 2.46 (s, 3H, CH_3), 3.16 (q, 2H, CH_2), 7.22 (t, 2H, HC$_{Ar}$), 7.29 (dd, 2H, HC$_{Ar}$), 7.53 (q, 2H, HC$_{Ar}$), 8.01 (s, 1H, HC$_{Ar}$). ^{13}C NMR (125 MHz, $CDCl_3$): δ = 13.62 (CH_3); 21.04 (CH_3); 26.76 (CH_2); 116.42 (CH_{Ar}); 116.61 (CH_{Ar}); 119.24 (HC$_{Ar}$); 125.92 (HC$_{Ar}$); 126.37 (HC$_{Ar}$); 130.93 (C$_{Ar}$); 131.00 (C$_{Ar}$); 131.78 (C$_{Ar}$); 135.69 (C$_{Ar}$); 135.91 (C$_{Ar}$); 145.76 (C$_{Ar}$); 155.96 (C); 161.80 (C); 163.98 (C).

5. Theoretical details

The DFT method at the B3LYP/6–311++G(d,p) theoretical level (Gaussian 16 package) is employed to optimise the ground state geometries of compounds **4a–d** (Frisch et al., 2016). Additionally, solvent effects and NMR chemical shifts (^{1}H and ^{13}C) were computed using the IEFPCM model (Tomasi et al., 2005) and the GIAO approach (Wolinski et al., 1990), respectively.

6. Biological evaluation

6.1. Cell culture

In this study, cancer cell lines were obtained from the company Sigma Aldrich. They were cultured under the following conditions: 37 °C, 5 % CO_2, and in a culture medium containing 1 % penicillin–streptomycin, 11 % fetal bovine serum, and MEM.

6.2. Molecular docking study

The bioactivity of compounds **4a–c** was evaluated against VEGFR-2/EGFR tyrosine kinase enzymes. These compounds demonstrated relatively good activity compared to the reference drug. Molecular docking was performed using the AutoDock package. The redocking of the original ligands in the active sites of two biological targets (EGFR: PDB 4ZAU, Yosaatmadja et al., 2015) and (VEGFR-2: PDB 4ASD, McTigue et al., 2012) was successfully reproduced, with RMSD values of 0.71 (for EGFR) and 1.49 (for VEGFR-2).

7. Results and discussion

The reaction steps followed in this study for synthesising compounds **4a–d** are presented in Scheme 1. Initially, 2-amino-5-methylbenzoic acid **1** underwent a substitution reaction with 4-fluorophenyl isothiocyanate **2** in the presence of base (triethylamine). The reflux process in ethanol yielded product **3** in substantial amounts. S-alkylation of product **3** with different acetamide derivatives or alkyl halide in acetone in the presence of K_2CO_3 constituted the second step of our synthesis, resulting in quinazolinone-based hybrids **4a–d**.

The structures of derivatives **3** and **4a–d** have been confirmed after performing several analytical techniques (^{1}H, ^{13}C NMR). For the quinazolinone products **4a–d**, their ^{1}H NMR spectra consistently show a

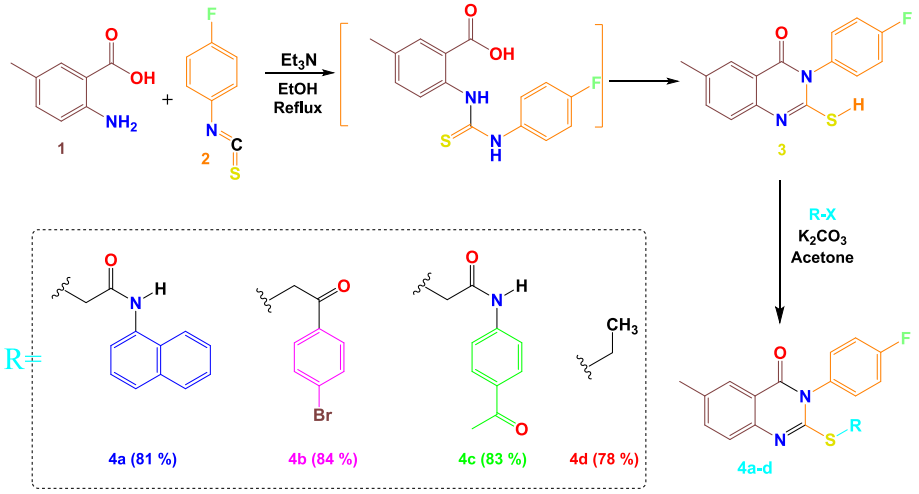

Scheme 1. Synthetic pathway adopted in the present work.

singlet corresponding to the CH_3 fragment attached to the quinazoline core, typically appearing around 2.50 ppm. In relation to the substituent added in the last stage of the synthesis process, singlet peaks have been detected at 10.19 and 10.87 ppm, corresponding to the protons carried on the NH atom in products **4a** and **4c**. Similarly, the ^{1}H NMR spectrum of compound **4d** reveals two distinct peaks: one appearing as a triplet at 1.35 ppm corresponding to the CH_3 group, and the other as a quadruplet at 3.15 ppm, attributed to the methylene protons (CH_2) directly attached to the sulfur atom. In addition, a multiplet is noted for the aromatic protons between 7.00 and 8.10 ppm. Further structural validation for products **4a–d** is provided by their ^{13}C NMR spectra, where a distinctive signal at 196.35 ppm relates to the carbonyl group (C = O) of the acetyl fragment located in the para position of product **4c**. On the other hand, the linker CH_2 in the case of products **4a–c** is identified in the range of 36.49–39.18 ppm. Moreover, the ^{13}C NMR spectrum for product **4d** provides confirmation of the suggested structure by the presence of two unique peaks at 13.62 and 26.76 ppm who are associated with the CH_3 and CH_2 of the sulphide group. Moreover, the ^{13}C NMR spectrum confirmed the absence of the thione (C = S) signal (for compound **3**), typically observed around 175 ppm. Instead, the resonance of the –N = C- was detected at 155.80 ppm for compound **3** and at δ 154.71–157.08 ppm for quinazolinone derivatives **4a–d**, corresponding to the chemical shift of the carbon atom (N = C), which suggests that compound 3 exists in its thiol form (Fig. 2) (Still et al., 1976).

7.1. NMR spectrum: Theoretical prediction

The chemical shifts found experimentally for NMR (^{1}H & ^{13}C) and those found theoretically are shown in Table 1. The optimised geometries with atomic numbering of **4a–d** are shown in Fig. 3. It should be noted that the predicted NMR (^{1}H & ^{13}C) chemical shifts of **4a–d** were obtained from their corresponding optimised geometries (Fig. 3).

Table 1
Chemical shift comparison (^{1}H NMR) of compounds **4a-d**.

	4a		4b		4c		4d	
	A	B	A	B	A	B	A	B
H1	7.82	8.04	8.06	8.02	8.15	7.99	7.93	8.01
H3	7.40	7.85	7.59	7.71	7.95	7.57	7.67	7.53
H4	7.19	7.66	7.52	7.49	7.87	7.76	7.49	7.53
H12	4.06	3.89	4.61	4.55	4.71	4.25	3.01	3.16
H13							1.41	1.35
H15	7.25	7.85	7.30	7.39	7.40	7.57	7.28	7.29
H16	7.20	7.52	7.27	7.30	7.37	7.72	7.25	7.22
H18	7.23	7.52	7.27	7.30	7.42	7.72	7.25	7.22
H19	7.32	7.85	7.30	7.39	7.45	7.57	7.28	7.29
H21	2.63	2.49	2.45	2.47	3.03	2.66	2.51	2.46
H34			8.06	7.98			–	
H35			7.52	7.14			–	
H37	7.65	7.30	7.54	7.71			–	
H38	7.41	7.20	7.93	7.98	8.60	8.07	–	
H39	8.03	7.30	–		8.04	7.87	–	
H40	7.93	7.60	–				–	
H41	7.57	7.20	–		8.01	7.87	–	
H42	7.52	7.20	–		6.91	8.07	–	
H43	7.88	7.60	–				–	
H45			–		2.34	2.55	–	

A: Prediected, B: Experimental.

Based on the values in Tables 1 and 2, a very high correlation was observed between the values obtained experimentally and theoretically across both spectra (^{1}H & ^{13}C)-NMR, with percentages ranging from 93.30 to 99.9 % and 96.00 to 99.9 %, respectively. The comparison of

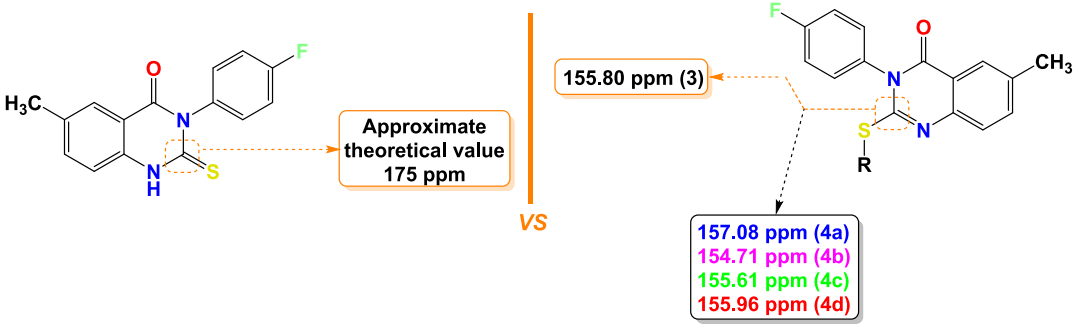

Fig. 2. Comparison at the ^{13}C NMR analysis level of the C2 of the starting compound **3** and the targeted compounds **4a–d**.

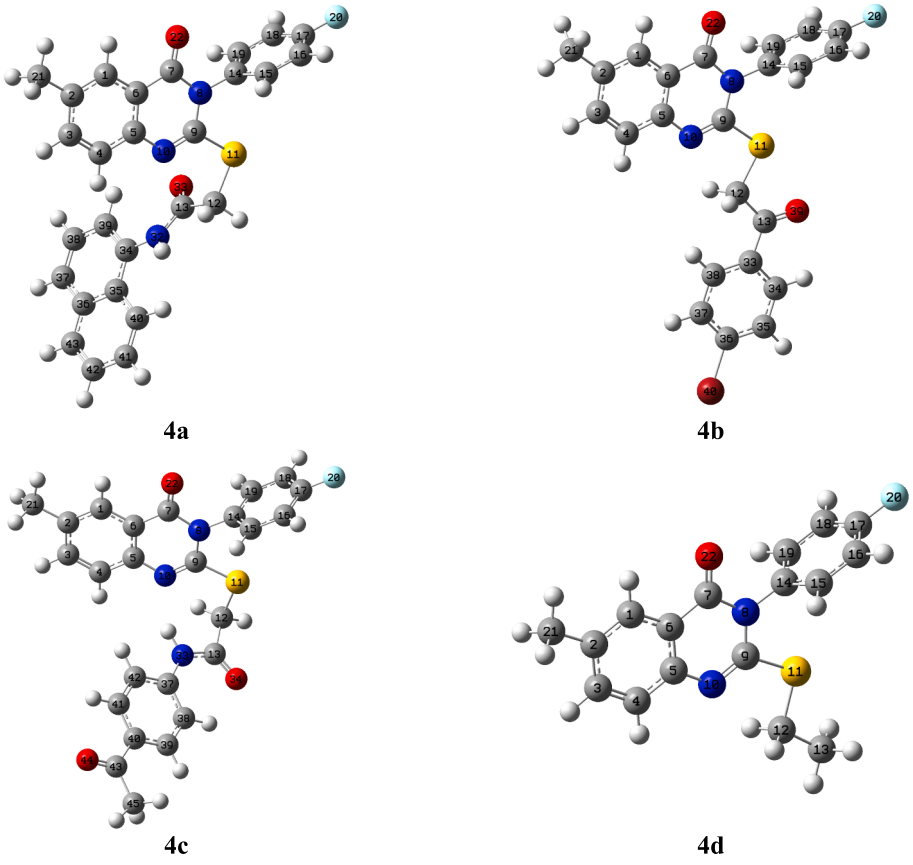

Fig. 3. The targeted compounds' geometric structures, following optimisation.

Table 2
Chemical shift comparison (^{13}C NMR) of compounds **4a-d**.

	4a		**4b**		**4c**		**4d**	
	A	B	A	B	A	B	A	B
C1	151.62	130.90	142.88	125.60	142.45	125.61	136.31	125.92
C2	165.12	161.00	158.93	136.26	155.54	135.61	148.07	135.91
C3	163.24	144.55	152.84	136.07	153.62	131.76	146.77	135.69
C4	151.33	130.82	141.94	119.25	140.89	119.11	136.44	126.37
C5	173.35	162.26	162.31	145.26	161.77	136.07	156.31	145.76
C6	143.83	119.35	135.01	116.92	134.77	118.18	129.33	119.24
C7	191.11	164.26	178.83	164.26	178.78	160.52	171.91	161.80
C9	189.62	157.08	177.55	154.71	179.81	155.61	171.96	155.96
C12	59.95	36.49	64.65	39.18	54.32	37.17	47.00	26.76
C13	195.48	166.84	211.69	192.69	186.22	196.35	21.02	13.62
C14	160.80	142.12	150.56	131.95	149.98	131.69	145.01	131.78
C15	159.07	136.72	149.08	131.95	148.86	129.40	143.13	130.93
C16	141.68	116.77	132.60	116.74	132.40	116.47	127.26	116.61
C17	196.28	196.72	150.90	135.02	184.00	166.32	176.31	163.98
C18	141.69	116.95	132.60	116.74	132.66	118.18	127.26	116.42
C19	159.20	136.72	149.07	131.08	148.86	129.40	143.13	131.00
C21	35.19	21.08	32.76	21.10	32.31	20.57	31.69	21.04
C33			148.94	131.02	–	–	–	–
C34	159.54	137.11	145.36	126.56	–	–	–	–
C35	151.13	129.38	148.36	129.86	–	–	–	–
C36	160.58	137.11	166.11	161.60	–	–	–	–
C37	150.30	124.74	148.03	129.86	161.07	143.12	–	–
C38	150.72	127.07	147.28	128.68	132.01	116.29	–	–
C39	143.49	116.95	–	–	148.75	129.40	–	–
C40	144.30	118.50	–	–	146.62	129.40	–	–
C41	151.98	132.54	–	–	144.26	125.78	–	–
C42	151.58	129.53	–	–	132.83	118.18	–	–
C43	154.94	132.45	–	–	169.72	145.03	–	–
C45		–	–	–	38.08	26.28	–	–

A: Prediected, B: Experimental.

values found for atoms H21 and H19 showed a difference of 0.1 ppm for compounds **4b** and **4d**.

Conversely, for hydrogen atom H42 in compound **4c**, a difference of 1.16 ppm was observed (Table 1). In the ^{13}C NMR spectrum, deviations between the observed chemical shifts and predicted ones are in ranges of 0–33.00, 4.00–22.4, 11.00–23.00, and 7.00–21.00 ppm for 4a, 4b, 4c, and 4d, respectively (Table 2).

8. Biological evaluation

8.1. Determining the cytotoxic potential

To evaluate the effect of quinazolinone products **4a–d** on the development of multiple cancer cell lines (A-549, MDA, and HeLa), a cytotoxicity assessment was carried out. The cytotoxic characteristics was analyzed through the MTT assay. The Docetaxel (a chemotherapy drug for treating different cancer types) serving as a positive control.

Products **4a–c** exhibited the strongest cytotoxic effects across all cell lines, with IC_{50} values between 0.49 ± 0.01 and 4.36 ± 0.09 μM. Product **4b** manifested an exceptionally strong cytotoxic activity against Hela, A-549, and MDA cell lines (ten times more active than the reference ''Docetaxel''), with IC_{50} values of 1.24 ± 0.03, 0.49 ± 0.01, and 1.07 ± 0.02 μM, respectively. Conversely, product **4d** displayed low potential to inhibit cancer cells, with elevated IC_{50} values of 48.5 ± 1.02 μM against HeLa cells and 46.3 ± 0.97 μM against A-549 cells. Nevertheless, derivative **4d** exhibited greater cytotoxicity against MDA cells, achieving an IC_{50} value of 5.75 ± 0.12 μM. Evaluation against A-549 cancer cells revealed excellent anticancer activity for derivatives **4a** and **4c**, with IC_{50} values of 1.31 ± 0.03 μM and 3.94 ± 0.08 μM, respectively. Conversely, these derivatives exhibited weaker anticancer effects against Hela cancer cells, with IC_{50} values of 3.48 ± 0.07 μM (**4a**) and 2.59 ± 0.05 μM (**4c**). Notably, significant cytotoxicity was observed against MDA cancer cells for both compounds.

8.2. In-vitro VEGFR-2 and EGFR kinase inhibitory assay

For the purpose of assessing the inhibitory activity of our synthesised products against EGFR, we specifically selected three compounds (**4a**, **4b** and **4c**) based on their potent cytotoxic profiles. The evaluation was conducted using an HTRF assay (El-Sattar et al., 2021). Docetaxel served as the standard with an IC_{50} of 56.1 ± 1.17 nM (Table 3). Compound **4c** exhibited significant EGFR inhibitory activity, closely resembling Docetaxel with an IC_{50} of 62.3 ± 1.47 nM. In comparison, Docetaxel had an IC_{50} of 56.1 ± 1.17 nM. Compound **4b**, a quinazoline derivative, also demonstrated notable EGFR inhibition with an IC_{50} of 68.2 ± 1.54 nM, showing a 12.1 nM difference compared to the reference. Additionally, compound **4a**, which features a naphthalene group substitution on the amide function, displayed moderate efficacy in EGFR inhibition, with an IC_{50} measured at 104 ± 2.18 nM, half as potent as Docetaxel in terms of cytotoxicity. In this assessment, we selected compounds **4a–c** (with high cytotoxic activities) tested against VEGFR-2 and EGFR according to the mechanism applied by Sogabe (Sogabe et al., 2013). Table 3 presents the IC_{50} values in nM (50 % inhibitory concentration). The tested derivatives exhibited excellent to good inhibitory activity, with IC_{50} values ranging from 90.1 ± 2.69 to 189 ± 5.66 nM for compounds **4a–c**. Compounds **4a** and **4c** demonstrated VEGFR-2 inhibition comparable to Docetaxel, with IC_{50} values of 92.2 ± 2.71 and 90.1 ± 2.69 nM, respectively. Conversely, compound **4b** exhibited moderate activity in front of VEGFR-2, with an IC_{50} of 189 ± 5.66 nM (approximately half as active as the reference).

Table 3
Cytotoxic activity of quinazoline products **4a–d** against Hela, A-549, and MDA cancer cells, also against EGFR and VEGFR-2 kinase assays for quinazoline derivatives **4a–c**.

Compound	IC_{50} [a,b]				
	Hela[a]	**A-549**[a]	**MDA**[a]	EGFR[b]	VEGFR-2[b]
4a	3.48 ±	1.31 ±	4.36 ±	104 ±	92.2 ±
4b	0.07	0.03	0.09	2.18	2.71
4c	1.24 ±	0.49 ±	1.07 ±	68.2 ±	189 ±
4d	0.03	0.01	0.02	1.54	5.66
Docetaxel	2.59 ±	3.94 ±	3.51 ±	**62.3 ±**	90.1 ±
	0.05	0.08	0.07	**1.47**	2.69
	48.5 ±	46.3 ±	5.75 ±	NT	NT
	1.02	0.97	0.12	56.1 ±	89.3 ±
	9.65 ±	10.8 ±	3.98 ±	1.17	2.67
	0.2	0.23	0.08		

[a] IC_{50} value (μM).
[b] IC_{50} values (nM).
[c]NT: Not tested compounds.

8.3. Molecular docking

To illustrate and understand the interesting cytotoxic profile observed for compounds **4a–c** against the targeted enzymes, a molecular docking analysis was conducted to identify the fragments of our products responsible for this activity, as well as assess the binding mode with the biological targets. Table 4 includes several parameters, such as the number of amino acids that can be incorporated into the complex formation between our products and the biological target, the binding energy of these complexes, and the number of hydrogen bonds.

The complexes formed between **4a–c** into the binding sites of the target enzymes show negative binding energies (BEs) in −7.11 and −9.21 kcal/mol (Table 4). The negative binding affinities of the stable complexes may explain the inhibitory efficiency of compounds **4a–c** towards the target enzymes (EGFR and VEGFR-2 kinase). However, BEs show slight differences. Thus, this parameter may not be used as a strong descriptor to explain the observed inhibition. Our focus will be on the type and number of interactions that may appear in the presence of the substituted groups of Sulphur atoms. Figs. 4 and 5 show the binding modes of derivatives **4a–c** into the binding sites of VEGFR2 and EGFR tyrosine kinases.

For EGFR, **4c** shows the highest inhibition efficiency followed by **4a** and **4b** with the lowest inhibition (*in-vitro*). The highest inhibition of **4c** is in good accordance with the number of interactions that form the N-(4-acetyl phenyl)acetamide fragment of compound **4c** into the binding site of EGFR tyrosine kinase compared to the ones established with N-(naphthalene-1-yl)acetylamide substituted group of **4a** and the substituted group 1-(4-bromophenyl)ethan-1-one of **4b** (Fig. 4). Indeed, N-(4-acetylphenyl)acetamide fragment of compound **4c** interacts with CYS A79 via hydrogen bond of GLY A796 and PRO A794 via carbon-hydrogen bond, and LEU A78 via π-σ interaction (Fig. 5). For VEGFR2 tyrosine kinase inhibition, the high inhibition efficiency of **4c** and **4a**

Table 4
Combining the values obtained from molecular docking (kcal/mol) and *in-vitro* tests of compounds **4a–c**.

Compound	Free binding energy	H-Bonds (HBs)	Number of amino acids *	IC_{50} ± SEM (nM)
VEGFR-2 kinase				
4a	−9.21	2	13	92.2 ± 2.71
4b	−7.75	3	14	189 ± 5.66
4c	−7.14	0	15	90.1 ± 2.69
Docetaxel				89.3 ± 2.67
EGFR				
4a	−7.54	1	9	104 ± 2.18
4b	−8.10	2	7	68.2 ± 1.54
4c	−7.11	1	7	62.3 ± 1.47
Docetaxel				56.1 ± 1.17

* Number of amino acids in the active site that show binding interaction with **4a-c**.

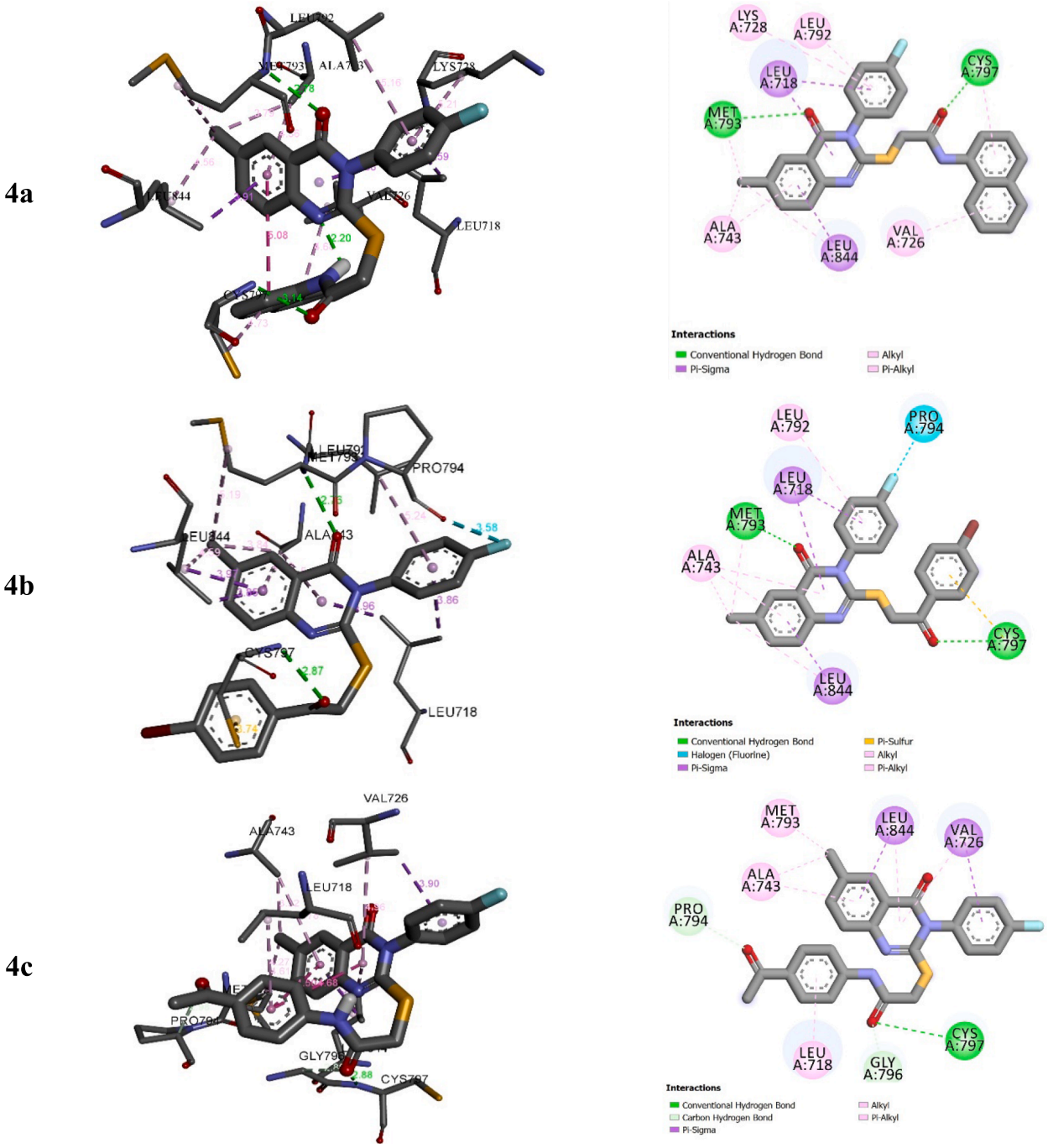

Fig. 4. Interactions between compounds **4a–c** and EGFR.

compared to **4b** may return to the π-sulphur interactions that formed with groups N-(4-acetylphenyl)acetamide and N-(naphthalen-1-yl) acetamide substituted groups in derivatives **4c** and **4a**, respectively (Fig. 5).

9. Conclusion

Four novel quinazoline derivatives were synthesised as dual VEGFR-2/EGFR inhibitors. Newly synthesised quinazolines were structurally characterised by NMR analyses. The cytotoxicity test showed that compound **4b** demonstrated the highest efficacy against A-549 cells, with an IC_{50} value of 0.49 ± 0.01 μM. Based on their cytotoxic performance, the inhibitory activity of products **4a–c** against EGFR and VEGFR-2 was assessed in subsequent evaluations. Notably, product **4c** proved to be the most potent, exhibiting an IC_{50} of 62.3 ± 1.47 nM against EGFR and 90.1 ± 2.69 nM against VEGFR-2. Studies involving molecular docking of product **4c** uncovered substantial interactions inside the active sites of VEGFR-2 and EGFR offering insights into its remarkable anticancer efficacy.

CRediT authorship contribution statement

Mohammed H. Geesi: Writing – review & editing, Writing – original draft, Visualization, Validation, Supervision, Software, Resources, Project administration, Methodology, Investigation, Funding acquisition, Formal analysis, Data curation, Conceptualization.

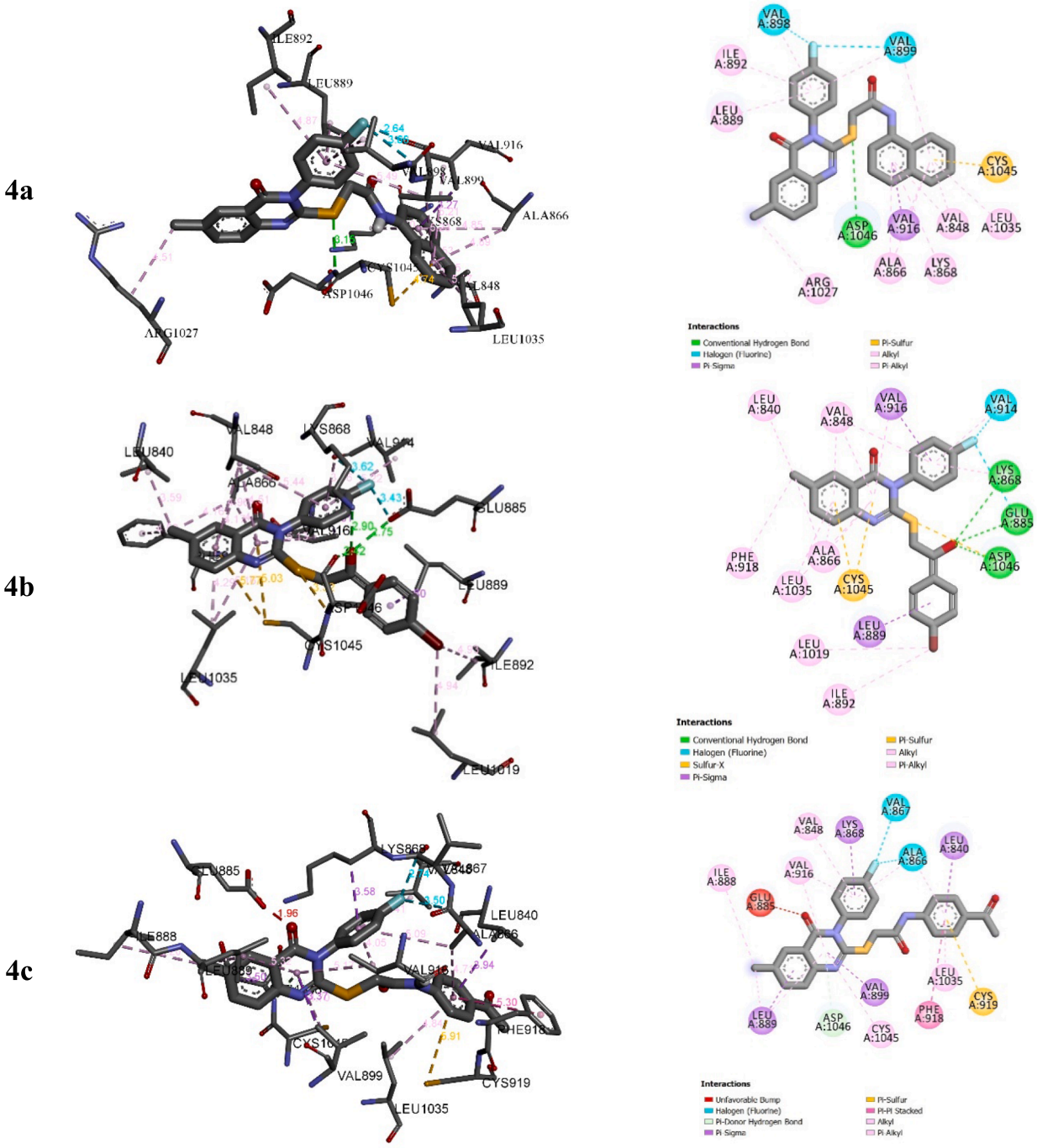

Fig. 5. Interactions between compounds **4a–c** and VEGFR-2.

Funding

"This study is supported *via* funding from Prince Sattam bin Abdulaziz University project number (PSAU/2024/R/1446) "

Declaration of competing interest

The authors declare that they have no known competing financial interests or personal relationships that could have appeared to influence the work reported in this paper.

Acknowledgement

"This study is supported *via* funding from Prince Sattam bin Abdulaziz University project number (PSAU/2024/R/1446) "

Appendix A. Supplementary data

Supplementary data to this article can be found online at https://doi.org/10.1016/j.jksus.2024.103518.

References

Abdullaziz, M.A., Abdel-Mohsen, H.T., El Kerdawy, A.M., Ragab, F.A., Ali, M.M., Abu-Bakr, S.M., Girgis, A.S., El Diwani, H.I., 2017. Design, synthesis, molecular docking

and cytotoxic evaluation of novel 2-furybenzimidazoles as VEGFR-2 inhibitors. Eur. J. Med. Chem. 136, 315–329. https://doi.org/10.1016/j.ejmech.2017.04.068.
Ayati, A., Moghimi, S., Salarinejad, S., Safavi, M., Pouramiri, B., Foroumadi, A., 2020. A review on progression of epidermal growth factor receptor (EGFR) inhibitors as an efficient approach in cancer targeted therapy. Bioorg. Chem. 99, 103811. https://doi.org/10.1016/j.bioorg.2020.103811.
Bray, F., Laversanne, M., Weiderpass, E., 2021. Soerjomataram I., The ever-increasing importance of cancer as a leading cause of premature death worldwide. CancerCancer 127 (16), 3029–3030. https://doi.org/10.1002/cncr.33587.
Byers, L.A., Heymach, J.V., 2007. Dual targeting of the vascular endothelial growth factor and epidermal growth factor receptor pathways: rationale and clinical applications for non-small-cell lung cancer. Clin. Lung. Cancer. 8, S79–S85. https://doi.org/10.3816/clc.2007.s.006.
Cao, Y., Arbiser, J., D'Amato, R.J., D'Amore, P.A., Ingber, D.E., Kerbel, R., Klagsbrun, M., Lim, S., Moses, M.A., Zetter, B., 2011. Forty-year journey of angiogenesis translational research. Sci. Transl. Med. 3, 114rv113. https://doi.org/10.1126/scitranslmed.3003149.
Cook, K.M., Figg, W.D., 2010. Angiogenesis inhibitors: current strategies and future prospects. CA Cancer J. Clin. 60 (4), 222–243. https://doi.org/10.3322/caac.20075.
Drakontaeidi, A., Papanotas, I., Pontiki, E., 2024. Multitarget pharmacology of sulfur-nitrogen heterocycles: anticancer and antioxidant perspectives. Antioxidants 13 (8), 898. https://doi.org/10.3390/antiox13080898.
El-Sattar, N.E.A., El-Adl, K., El-Hashash, M.A., Salama, S.A., Elhady, M.M., 2021. Design, synthesis, molecular docking and in silico ADMET profile of pyrano [2,3-d] pyrimidine derivatives as antimicrobial and anticancer agents. Bioorg. Chem. 115, 105186. https://doi.org/10.1016/j.bioorg.2021.105186.
Frisch, M J., Trucks G.W., Schlegel H.B., Scuseria G.E., Robb M.A., Cheeseman J.R., Scalmani G., Barone V., Petersson G.A., Nakatsuji H., Li X., Caricato M., Marenich A. V., Bloino J., Janesko B.G., Gomperts R., Mennucci B., Hratchian H.P, Ortiz J.V., Izmaylov A.F., Sonnenberg J.L., Williams., Ding F., Lipparini F., Egidi F., Goings J., Peng B., Petrone A., Henderson T., Ranasinghe D., Zakrzewski V.G., Gao J., Rega N., Zheng G., Liang W., Hada M., Ehara M., Toyota K., Fukuda R., Hasegawa J., Ishida M., Nakajima T., Honda Y., Kitao O., Nakai H., Vreven T., Throssell K., Montgomery J.r.. J A., Peralta J.E., Ogliaro F., Bearpark M.J., Heyd J.J., Brothers E.N., Kudin K.N., Staroverov V.N., Keith T.A., Kobayashi R., Normand J., Raghavachari K., Rendell A. P., Burant J.C., Iyengar S.S., Tomasi J., Cossi M., Millam J.M., Klene M., Adamo C., Cammi R., Ochterski J.W., Martin R.L., Morokuma K., Farkas O., Foresman J.B., Fox D.J., Gaussian 16 Rev. C.01, Wallingford, CT, 2016.
Geesi, M.H., 2020. Synthesis, antibacterial evaluation, Crystal Structure and Hirshfeld surface analysis of a new 2-Benzylsulfanyl-3-(4-fluoro-phenyl)-6-methyl-3H-quinazolin-4-one. J. Mol. Str. 1208, 127894. https://doi.org/10.1016/j.molstruc.2020.127894.
Geesi, M.H., Riadi, Y., Kaiba, A., Ouerghi, O., Ibnouf, E.O., Guionneau, P., 2020. Synthesis, antibacterial evaluation, raman, crystal structure and hirshfeld surface analysis of a new 3-(4-fluorophenyl)-6-methyl-2-(propylthio) quinazolin-4 (3H)-one. J. Mol. Str. 1215, 128265. https://doi.org/10.1016/j.molstruc.2020.128265.
Ghorab, M.M., Alsaid, M.S., Soliman, A.M., Ragab, F.A., 2017. VEGFR-2 inhibitors and apoptosis inducers: synthesis and molecular design of new benzo[g]quinazolin bearing benzenesulfonamide moiety. J. Enzyme. Inhib. Med. Chem. 32, 893–907. https://doi.org/10.1080/14756366.2017.1334650.
Ghorab, M.M., Alsaid, M.S., Soliman, A.M., 2018. Dual EGFR/HER2 inhibitors and apoptosis inducers: New benzo-quinazoline derivatives bearing benzenesulfonamide as anticancer and radiosensitizers. Bioorg. Chem. 80, 611–620. https://doi.org/10.1016/j.bioorg.2018.07.015.
Gschwind, A., Fischer, O.M., Ullrich, A., 2004. The discovery of receptor tyrosine kinases: targets for cancer therapy. Nat. Rev. Cancer 4 (5), 361–370. https://doi.org/10.1038/nrc1360.
Kumar, A., Singh, A.K., Singh, H., Vijayan, V., Kumar, D., Naik, J., Thareja, S., Yadav, J. P., Pathak, P., Grishina, M., Verma, A., Khalilullah, H., Jaremko, M., Emwas, A., Kumar, P., 2023. Nitrogen containing heterocycles as anticancer agents: a medicinal chemistry perspective. Pharmaceuticals 16 (2), 299. https://doi.org/10.3390/ph16020299.
Lee, K., Jeong, K.-W., Lee, Y., Song, J.Y., Kim, M.S., Lee, G.S., Kim, Y., 2010. Pharmacophore modeling and virtual screening studies for new VEGFR-2 kinase inhibitors. Eur. J. Med. Chem. 45, 5420–5427. https://doi.org/10.1016/j.ejmech.2010.09.002.
Li, S.-N., Li, H.-Q., 2014. Epidermal growth factor receptor inhibitors: a patent review (2010–present). Expert Opin. Ther. Pat. 24 (3), 309–321. https://doi.org/10.1517/13543776.2014.871527.
Liu, Y.i., Gray, N.S., 2006. Rational design of inhibitors that bind to inactive kinase conformations, Nat. Chem. Biol. 2 (7), 358-364.doi: 10.1038/nchembio799.
Liu, Q., Yu, S., Zhao, W., Qin, S., Chu, Q., Wu, K., 2018. EGFR-TKIs resistance via EGFRindependent signaling pathways. Mol. Cancer. 17, 1–9. https://doi.org/10.1186/s12943-018-0793-1.
Martins, P., Jesus, J., Santos, S., Raposo, L.R., Roma-Rodrigues, C., Baptista, P.V., Fernandes, A.R., 2015. Heterocyclic anticancer compounds: recent advances and the paradigm shift towards the use of nanomedicine's tool box. Molecules 20 (9), 16852–16891. https://doi.org/10.3390/molecules200916852.
McTigue M, Murray B W, Chen J H, Deng Y-L, Solowiej J, Kania R S., 2012. Molecular conformations, interactions, and properties associated with drug efficiency and clinical performance among VEGFR TK inhibitors. Proceedings of the National Academy of Sciences. 109:18281-18289. doi: 10.1073/pnas.1207759109.
Obaid, R.J., Naeem, N., Mughal, E.U., Al-Rooqi, M.M., Sadiq, A., Jassas, R.S., Moussa, Z., Ahmed, S.A., 2022. Inhibitory potential of nitrogen, oxygen and sulfur containing heterocyclic scaffolds against acetylcholinesterase and butyrylcholinesterase. RSC Adv. 12 (31), 19764–19855. https://doi.org/10.1039/D2RA03081K.
Panigrahy, D., Singer, S., Shen, L.Q., Butterfield, C.E., Freedman, D.A., Chen, E.J., Moses, M.A., Kilroy, S., Duensing, S., Fletcher, C., 2002. PPARγ ligands inhibit primary tumor growth and metastasis by inhibiting angiogenesis. J. Clin. Investig. 110, 923–932. https://doi.org/10.1172/JCI15634.
Panigrahy, D., Huang, S., Kieran, M.W., Kaipainen, A., 2005. PPARγ as a therapeutic target for tumor angiogenesis and metastasis. Cancer Biol. Ther. 4 (7), 687–693. https://doi.org/10.4161/cbt.4.7.2014.
Papanotas, I., Pontiki, E., 2024. Multitarget Pharmacology of Sulfur-Nitrogen Heterocycles: Anticancer and Antioxidant Perspectives. Antioxidants 13 (8), 898. https://doi.org/10.3390/antiox13080898.
Peerzada, N., Hamel, E., Bai, R., Supuran, C.T., Azam, A., 2021. Deciphering the key heterocyclic scaffolds in targeting microtubules, kinases and carbonic anhydrases for cancer drug development. Pharmacol. Ther. 225, 107860. https://doi.org/10.1016/j.pharmthera.2021.107860.
Riadi, Y., Geesi, M.H., Ejaz, S.A., Afzal, O., Oubella, A., 2024. Design, characterization, and DFT exploration of new quinazoline-N-substituted analogs: Anti-cancer activity and molecular docking insights. J. Mol. Str. 140420. https://doi.org/10.1016/j.molstruc.2024.140420.
Sogabe, S., Kawakita, Y., Igaki, S., Iwata, H., Miki, H., Cary, D.R., Takagi, T., Takagi, S., Ohta, Y., Ishikawa, T., 2013. Structure-based approach for the discovery of pyrrolo [3, 2-d] pyrimidine-based EGFR T790M/L858R mutant inhibitors. ACS Med. Chem. Lett. 4 (2), 201–205. https://doi.org/10.1021/ml300327z.
Soliman, A.M., Alqahtani, A.S., Ghorab, M.M., 2019. Novel sulfonamide benzoquinazolinones as dual EGFR/HER2 inhibitors, apoptosis inducers and radiosensitizers. J. Enzyme Inhib. Med. Chem. 34 (1), 1030–1040. https://doi.org/10.1080/14756366.2019.1609469.
Still, I.W.J., Plavac, N., McKinnon, D.M., Chauhan, M.S., 1976. Carbon-13 nuclear magnetic resonance spectra of organic sulfur compounds. Substituent chemical shift (scs) effects in the 4-thiazoline-2-thione series. Can. J. Chem. 54 (10), 1660–1664. https://doi.org/10.1139/v76-235.
Stockley, T., Souza, C.A., Cheema, P.K., Melosky, B., Kamel, S., Tsao, M.S., Spatz, A., Karsan, A., 2018. Evidence-based best practices for EGFR T790M testing in lung cancer in Canada. Curr. Oncol. 25 (2), 163–169. https://doi.org/10.3747/co.25.4044.
Tilahun, M., Laamari, Y., Irfan, A., Oubella, A., Alossaimi, M.A., Riadi, Y., Morjani, H., Auhmani, A., Itto, M.Y.A., 2025. New isoxazoline-linked 1,3,4-thiadiazole derivatives: synthesis, antiproliferative activity, molecular docking, molecular dynamics and DFT. J. Mole. Str. 1319, 139368. https://doi.org/10.1016/j.molstruc.2024.139368.
Tomasi, J., Mennucci, B., Cammi, R., 2005. Quantum mechanical continuum solvation models. Chem. Rev. 105, 2999–3094. https://doi.org/10.1021/cr9904009.
Traxler, P., Furet, P., 1999. Strategies toward the design of novel and selective protein tyrosine kinase inhibitors, Pharmacol. Ther. 82, 195-206. doi: 10.1016/s0163-7258(98)00044-8.
Wolinski, K., Hinton, J.F., Pulay, P., 1990. Efficient implementation of the gauge-independent atomic orbital method for NMR chemical shift calculations. J. Am. Chem. Soc. 112, 8251–8260. https://doi.org/10.1021/ja00179a005.
Ying, Y., Lei, S., Yang, Z., Huan-Qiu, L., Zhen-Wei, Z., Hai-Liang, Z., 2010. Design, synthesis and biological evaluation of quinoline amide derivatives as novel VEGFR-2 inhibitors. Bioorg. Med. Chem. Lett. 20 (22), 6653–6656. https://doi.org/10.1016/j.bmcl.2010.09.014.
Yosaatmadja, Y., Silva, S., Dickson, J.M., Patterson, A.V., Smaill, J.B., Flanagan, J.U., Mckeage, M.J., Squire, C.J., 2015. Binding mode of the breakthrough inhibitor AZD9291 to epidermal growth factor receptor revealed. J. Stru. Bio. 192, 539–544. https://doi.org/10.1016/j.jsb.2015.10.018.
Yu, H.A., Pao, W., 2013. Afatinib-new therapy option for EGFR-mutant lung cancer. Nat. Rev. Clin. Oncol. 10 (10), 551–552. https://doi.org/10.1038/nrclinonc.2013.154.
Zahran, S.S., Ragab, F.A., El-Gazzar, M.G., Soliman, A.M., Mahmoud, W.R., Ghorab, M. M., 2023. Antiproliferative, antiangiogenic and apoptotic effect of new hybrids of quinazoline-4(3H)-ones and sulfachloropyridazine. Eur. J. Med. Chem. 245, 114912. https://doi.org/10.1016/j.ejmech.2022.114912.